PHYSICAL REVIEW B **91**, 220301(R) (2015)

Broadband perfect absorption of ultrathin conductive films with coherent illumination: Superabsorption of microwave radiation

Sucheng Li,[1] Jie Luo,[1] Shahzad Anwar,[1] Shuo Li,[1] Weixin Lu,[1] Zhi Hong Hang,[1] Yun Lai,[1] Bo Hou,[1,*] Mingrong Shen,[1] and Chinhua Wang[1,2]

[1]*College of Physics, Optoelectronics and Energy & Collaborative Innovation Center of Suzhou Nano Science and Technology, Soochow University, 1 Shizi Street, Suzhou 215006, China*

[2]*Jiangsu Key Lab of Advanced Optical Manufacturing Technologies, Soochow University, 1 Shizi Street, Suzhou 215006, China*

(Received 12 June 2014; revised manuscript received 17 May 2015; published 11 June 2015)

Absorption of microwaves by metallic conductors is typically inefficient, albeit naturally broadband, due to the huge impedance mismatch between metal and free space. Reducing metal to ultrathin profile may improve absorption efficiency, but a maximal 50% absorption limit induced by the field continuity exists. Here, we experimentally show that broadband, perfect (100%) absorption of microwaves can be realized in a single layer of ultrathin conductive film when illuminated coherently by two oppositely directed incident beams. Our experiments keep the field continuity and simultaneously break the 50% limit. Inheriting the intrinsic broadband feature of metals, complete absorption is observed to be frequency independent in microwave experiments from 6 to 18 GHz. Remarkably, this occurs in films with thicknesses that are at the extreme subwavelength scales, $\sim\lambda/10\,000$ or less. Our work proposes a way to achieve total electromagnetic wave absorption in an ultrawide spectrum of radio waves and microwaves with a simple conductive film.

DOI: 10.1103/PhysRevB.91.220301 PACS number(s): 41.20.Jb, 42.25.Bs, 78.20.−e, 84.40.−x

I. INTRODUCTION

The dissipation of microwaves in metallic conductors is negligibly small, although the free-carrier absorption is broadband in nature due to the absence of the bounding force for the free carriers [1]. From an impedance point of view, a huge mismatch exists between the metal and free space. By reducing the thickness, the ultrathin conductive film of conductivity, σ, and thickness, h, may absorb electromagnetic (EM) waves in a frequency-independent manner because of the improved match between the film impedance (i.e., sheet resistance $R_s = 1/\sigma h$ in the ultrathin case, measuring the in-plane resistance for a film of arbitrarily sized square shape, also expressed in *ohms per square*) and the vacuum impedance Z_0 [2–6]. However, the absorption is restricted to 50% maximum, whatever R_s is [2–6]. It has been assumed that the 50% limit cannot be broken under the ultrathin approximation, where $h \ll \delta$ (skin depth) and hence the parallel component of the electric field (E field) is continuous across the film. This limit severely compromises the appealing properties of inherent broadband and ultrathin scale when using conductive thin film as an absorber.

Since a broadband ultrathin perfect absorber is highly desirable in numerous applications from microwave to infrared and visible wavelengths [7–10], various design strategies have been proposed, such as using thick substrates or lossy elements [3,9–10], composite structures/materials [2,11–14], local resonances [15–20], and functional reflection boundaries [21–24], where the field continuity is not applicable due to either phase accumulation or resonance or reflection boundary. Consequently, the absorption can be enhanced up to 100%, but the resultant absorber either becomes bulky if its performance is broadband, or requires complicated fabrication and is a perfect absorber only over a narrow band if its thickness is subwavelength. The relative bandwidths, $2(f_u - f_l)/(f_u + f_l)$, where f_u and f_l are the upper and lower frequencies of the perfect absorption band, among the experimentally demonstrated perfect absorbers, are usually less than 100% and do not approach the limiting value of 200% ($f_l \to 0$ and/or $f_u \to \infty$) [7–24].

A new concept called coherent perfect absorption (CPA) has attracted a lot of research interest recently [25–34]. Regarded as the time-reversal process of laser generation, CPA takes place when a Fabry-Perot (FP) dielectric cavity is illuminated by two counterpropagating coherent light beams, and all input EM energy is trapped and dissipated inside the cavity, accomplishing 100% absorption. Originally with the FP cavity, the optical CPA operates at a specific frequency and the wavelength thick material. Very recently, metallic film CPA was investigated theoretically, demonstrating an unparalleled bandwidth and thin-profile advantages [30].

In this Rapid Communication, we experimentally demonstrate that the broadband perfect absorption with relative bandwidth of 100% can be realized in ultrathin conductive films illuminated coherently by two opposite microwave beams. The films are transparent conductors [35–43] with conducting layer thickness, i.e., absorbing thickness of $\sim\lambda/10\,000$ (λ denoting the wavelength in vacuum). Such thin films maintain the field continuity required for EM waves to travel across themselves, and hence do not bring about a phase shift, in sharp contrast to previous perfect absorber designs. The coherent illumination increases the film absorbance to 100% in a frequency-independent manner, which implies ultrabroadband behavior in the spectrum of radio waves and microwaves. This extremely subwavelength-scale, inherently broadband, perfect absorption not only breaks the 50% dissipation limit, but is also simple in design and exhibits superabsorption.

II. BROADBAND PERFECT ABSORPTION

It is known that the 50% optimal absorption depends solely on the sheet resistance, requiring $R_s = Z_0/2 = 188\,\Omega$

*Corresponding author: houbo@suda.edu.cn

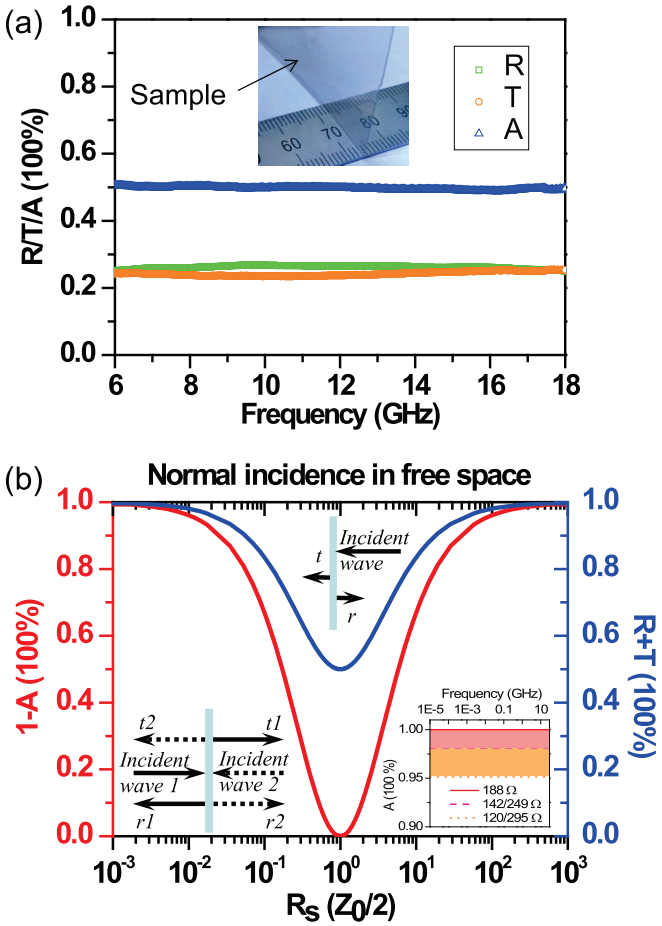

FIG. 1. (Color online) Fifty percent absorption limit and the frequency-independent perfect absorption. (a) Normal reflectance, transmittance, and absorbance of the ultrathin conductive film, with sheet resistance 180 Ω. Inset is the photo of the sample, where the underlying ruler has the minimum division of 1 *millimeter*. (b) Effect of the sheet resistance on the reflectance and transmittance in two cases: the single-beam illumination (upper inset, blue curve, and right axis) and the coherent illumination (left inset, red curve, and left axis). Right inset with the logarithmic scale of frequency illustrates the frequency independency of the broadband absorption, where three absorbance curves denoted by the sheet resistances are calculated according to Eq. (1), where the shading area represents $A \geqslant 95\%$ for $120\,\Omega \leqslant R_s \leqslant 295\,\Omega$, the red area represents $A \geqslant 98\%$ for $142\,\Omega \leqslant R_s \leqslant 249\,\Omega$, and $A = 100\%$ for $R_s = 188\,\Omega$.

at normal incidence, and can be observed in various smooth or structured thin films, regardless of their compositions [2–6]. Transparent conductors, which are conducting layers with excellent optical transparency, are an important type of optoelectronic material that can be produced using various technological approaches [38–43]. In applications, conducting layers are supported by transparent substrates and their electrical characterization is specified in terms of R_s. In this work, the customized commercial transparent conductive films with a 2.6-μm-thick conducting layer and a 0.2-mm-thick polymer substrate are employed (see Supplemental Material A for details on the sample [44]). The $R_s = 180\,\Omega$ film sample, illustrated by the inset of Fig. 1(a), is inserted into the microwave passage for measuring the reflection/transmission coefficients, r/t (see Supplemental Material B [44]). The absorbance is calculated from $A = 1 - R - T$, where the reflectance $R = |r|^2$ and the transmittance $T = |t|^2$. The measured results at normal incidence are plotted in Fig. 1(a), which shows 50% absorption.

At optimal absorption with the ideal condition $R_s = Z_0/2$, the transmission and reflection coefficients are $t = 0.5$ and $r = -0.5$, respectively. In this situation, we launch the second beam at the other side, which has the same amplitude, phase, and polarization as the first one in terms of E field, depicted schematically by the left inset in Fig. 1(b). Then, the second beam has the transmission $t2 = 0.5$, completely canceling the first beam reflection $r1 = -0.5$. Likewise, perfect cancellation happens at the right side for $t1$ and $r2$. A straightforward calculation proves that the incident power per unit area from two beams, $2 \times 0.5|E_0|^2/Z_0$ (E_0 denoting the incident E field), is equal to the film's resistive heating per unit area, $0.5\ \mathrm{Re}[JE^*]h = 0.5|E_0|^2/R_s$ (the induced current $J = \sigma E$, the E field in the film $E = E_0$ due to the field continuity, and $R_s = Z_0/2$). Thus, the total incident energy is entirely deposited on the film and dissipated by the free carriers, which is just the CPA.

From the analytical calculation (see Supplemental Material C [44]), the reflectance in the coherent illumination is

$$R = |1 - (0.5Z_0/R_s)|^2/|1 + (0.5Z_0/R_s)|^2. \qquad (1)$$

Here, the signals, $r1$, $t1$, $r2$, and $t2$ are considered as reflection, and the absorbance is calculated to be $1 - R$. Figure 1(b) shows the calculated quantity $1 - A$ with varying the sheet resistance in the two cases at normal incidence. $R = 0 (A = 1)$ is seen at $R_s = Z_0/2$ for the coherent illumination, whereas the absorbance is only 50% under the single-beam case. In particular, both Eq. (1) and the CPA condition, $R_s = 1/\sigma h = Z_0/2$, show no physical quantities dependent on frequency, if σ is nondispersive. This reveals the frequency-independent absorption behavior that is robust in the radio/microwave regime, where the dc conductivity is applicable, and may deteriorate in the terahertz (THz) domain, where σ becomes dispersive. Therefore, Fig. 1(b) is not specific to some frequency, but general in a broadband spectrum of radio waves and microwaves, as illustrated explicitly by the right inset. Note that >98% absorbance can be obtained while R_s ranges extensively from 142 to 249 Ω, which indicates the resistance insensitivity.

The basic difference between the optical CPA and our case is the material system. In the former, a high-Q resonant cavity made of low-loss semiconductors is necessary for the antilasering process, and thus leads inevitably to selecting the working frequency from the cavity size and the sensitivity to material parameters in terms of dispersive permittivity or refractive index. In our case, no cavity is involved, and the lossy film is nonresonant, which is very beneficial to ultrabroadband applications. Furthermore, in our discussed spectrum range where both ultrathin ($h \ll \delta$) and low-frequency [$\sigma/(\omega\varepsilon_0) \gg 1$] conditions hold, the dimensional and material parameters of the film can be combined into a single nondispersive characteristic quantity, R_s, which has explicit meaning in physics and great utility in engineering applications (see the use of the impedance language in Supplemental Material C [44]).

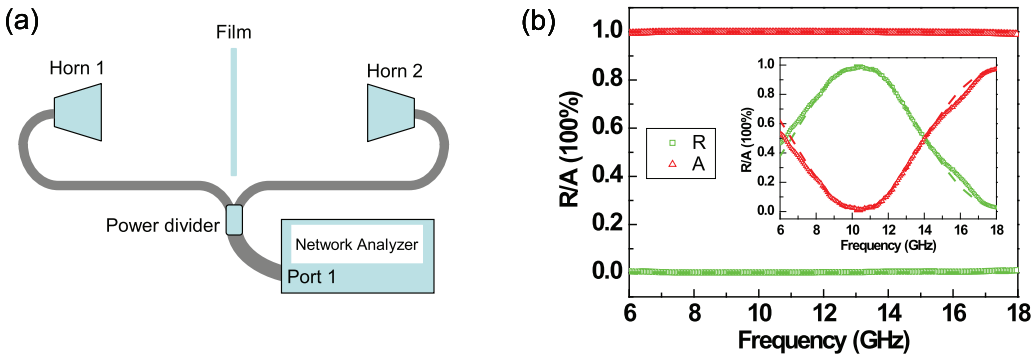

FIG. 2. (Color online) Coherent perfect absorption in free space. (a) Schematic drawing of the experimental setup in free space. (b) Measured (open symbols) and calculated (dashed lines) results in free space for the cases of $L = 0$ and $L = 14.5$ mm (inset). L denotes the difference in the distance of the film to the two horn antennas. The sample has the sheet resistance 180 Ω.

III. RESULTS AND DISCUSSION

The coherently illuminating experiment was first implemented in free space using the setup shown schematically in Fig. 2(a). Two identical rectangular horn antennas are connected with port 1 of the microwave network analyzer using identical coaxial cables and a −3 dB power divider [45]. The sample is first inserted in the proper position with the identical separations to the antennas, i.e., the distance difference is $L = 0$. In this symmetrical configuration, the two incident waves emitted from the horns satisfy the in-phase relationship, i.e., the relative phase is $\Delta\varphi = 0$. The measured and calculated results are plotted in Fig. 2(b), where the measured absorbance is >99% over the experimental range, 6–18 GHz, with a mean value of 99.6% (see Supplemental Material B for details on the free space measurement [44]). This complete absorption is seen to be frequency independent, corresponding to a 100% relative bandwidth. In principle, the lower frequency, f_l, of the perfect absorption band can be close to 0 Hz and the relative bandwidth will approach 200%. As discussed, the native broadband feature comes from the nondispersive conductivity and is an intrinsic consequence of free carriers dissipating the EM wave of low frequencies. In particular, note that the efficient dissipating layer is only ∼3 μm thick, which is extremely subwavelength (∼$\lambda/10\,000$) and much less than δ (see Supplemental Material D for the EM parameters of the film [44]).

If the distances of the film to the antennas are adjusted so that L is nonzero, say 14.5 mm, the experimental spectra show a ∼0 absorption minimum, as plotted in the inset of Fig. 2(b). This zero absorption is related to $\Delta\varphi$. When $\Delta\varphi = k_0 L = m\pi$ ($k_0 = 2\pi f/c$, where f is the frequency, c the speed of light in vacuum, and m is an odd integer) at a specific frequency, the E fields of the two waves cancel each other out at the sample position, no free-carrier dissipation is induced, and consequently there is no absorption at all. The frequency of zero absorption, 10.5 GHz, is in good agreement with the condition $k_0 L = \pi$.

The CPA can also take place for oblique incidence. In Fig. 3(a), the two beams are incident at the same oblique angle θ_0. Likewise, due to the mutual cancellation of the reflected and transmitted beams on either side, 100% of the EM energy carried by the dual oblique beams is trapped in the conductive film and finally dissipated as ohmic loss. The reflectances for both TM and TE incidences are calculated and plotted in Figs. 3(b) and 3(c), where the green line denotes the zero reflectance condition, $R_s = (Z_0/2)\cos\theta_0$ (TM) and $R_s = (Z_0/2)/\cos\theta_0$ (TE). These two conditions do not depend on frequency either. With the $Z_0/2$ sheet resistance, the angular tolerance for >90% TM and TE absorbance is as large as 60°. Instead of measuring absorption for oblique incidence in free space with four horn antennas, we performed the measurement inside a rectangular waveguide. The difference is θ_0 changes with frequency according to $\cos\theta_0 = \beta/k_0$, where β is the propagation constant of the waveguide mode.

In the waveguide experiment, the sample is sandwiched between two identical X band coax-to-waveguide adapters, and the TE10 mode is launched from both sides and travels toward the sample with the same phase, as illustrated in the inset in Fig. 3(d) (see Supplemental Material B for details on the waveguide measurement [44]). To make the waveguide in single mode, measurements are carried out below the TE20 cutoff of 13 GHz. The magenta triangles are the result of the $R_s = 221\,\Omega$ sample, and indicate the absorption increases from 84% at 7 GHz to 99% beyond 10 GHz. In an alternative view, the TE10 mode can be decomposed as two TEM beams propagating at the same oblique angle $\theta_0 = \cos^{-1}(\beta/k_0)$, which implies θ_0 decreases with frequency. Therefore, the magenta triangles curve is consistent with the angular variation of the reflectance at $R_s = 221\,\Omega$ in Fig. 3(c).

The $R_s = 442\,\Omega$ sample is also tested in our waveguide setup, seeing the red circles in Fig. 3(d). It is noted that the absorbance is greater than 90% over the X band, and the nearly full absorption, 99.6%, appears around 7.35 GHz, labeled as "A" in Fig. 3(d). As shown in Fig. 3(c), the perfect absorption for $R_s = 442\,\Omega$ occurs to $\theta_0 = 64°$, also labeled, which matches the 7.35 GHz TE10 mode. The calculated results of the two samples, plotted as lines in Fig. 3(d), agree well with the measured ones. Therefore, the waveguide experiment proves that the CPA persists to the off-normal incidence, if the sheet resistance changes accordingly. In fact, the prerequisite of the oblique CPA, which likewise is $t^{\mathrm{TE(TM)}} = 0.5$ and $r^{\mathrm{TE(TM)}} = -0.5$ at single-beam illumination, can be obtained from Eq. (S1), which depends on both θ_0 and R_s, in Supplemental Material C [44].

The relative phase of the two TE10 beams when reaching the sample can be controlled by adding the delay line, e.g., a

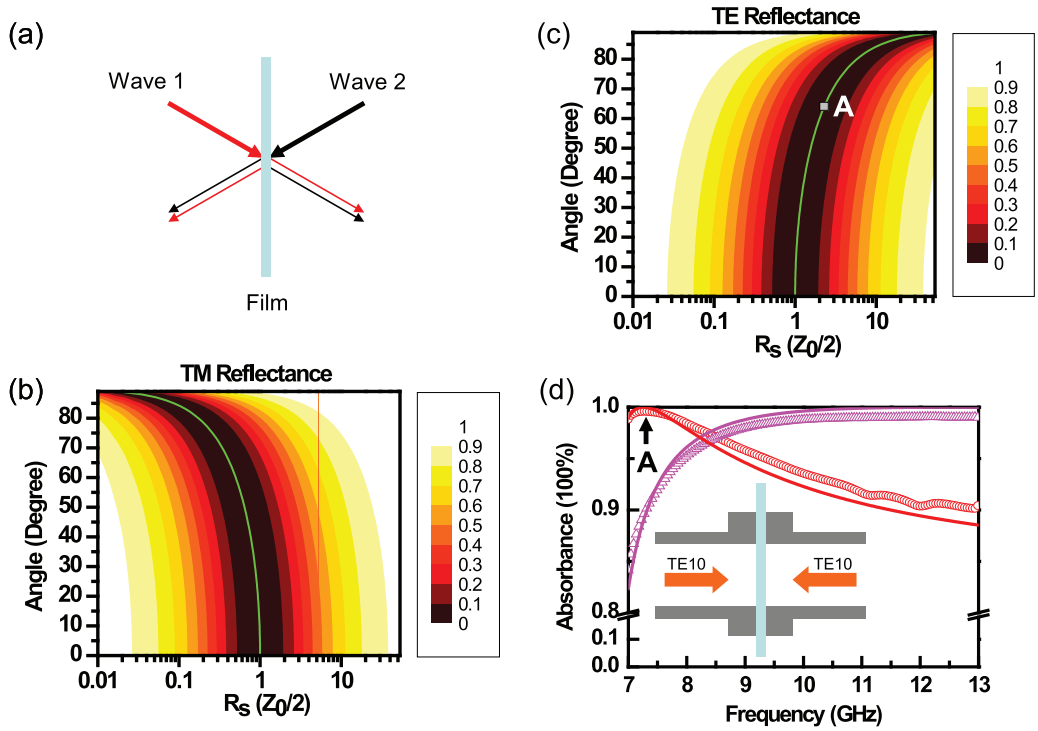

FIG. 3. (Color online) Coherent perfect absorption in oblique incidences. (a) Schematic drawing of the CPA at oblique angle θ_0. (b) and (c) Calculated reflectance under TM and TE illumination, respectively, where the green line denotes the CPA condition, $R_s = (Z_0/2)\cos\theta_0$ (TM) and $R_s = (Z_0/2)/\cos\theta_0$ (TE). (d) Measured (symbols) and calculated (lines) results in the X band waveguide, as illustrated schematically by the inset. The samples have the sheet resistance 221 Ω (magenta triangles and line) and 442 Ω (red circles and line).

section of waveguide (length $L = 140$ mm), to the passage of one beam. It can be inserted at either side of the sample, and the phase delay introduced is βL. (For general tunability, a phase shifter may provide arbitrary phase control.) In Fig. 4, we show the measured and calculated absorbance (green symbols for the left insertion, magenta symbols for the right, and the solid line for the calculation). As expected, the curves agree very well and reveal the rapid modulation of absorption within the X band. Interestingly, the absorption twin peaks appear and evolve into the bands with frequency. These bands as well

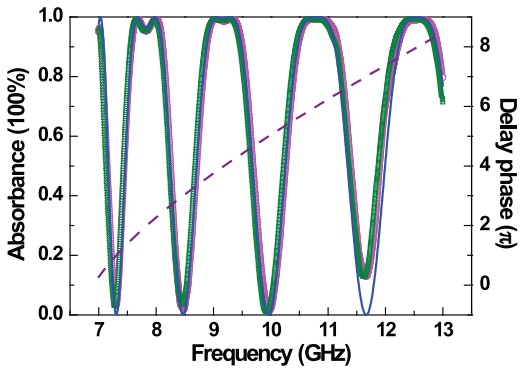

FIG. 4. (Color online) Coherent perfect absorption in the waveguide with large phase delay. Measured (open symbols: green for the left addition and magenta for the right addition) and calculated (solid line) absorbance in the waveguide with the addition of the $L = 140$-mm-long delay line. Dashed line denotes the delay phase βL, and is associated with the right axis. The sample has the sheet resistance 221 Ω.

as the absorption minima are associated with $\Delta\varphi = \beta L = m\pi$ (the even number m for the band center and the odd m for the minima), as indicated by the dashed line in Fig. 4. The formula (see Supplemental Material C [44]) reveals that the twin peak is from $(Z_0/2)\cos(\Delta\phi)/(R_s\cos\theta_0) = 1$, which conditionally holds at two frequencies around $\Delta\varphi = m\pi$ (m being the even number) relying on the parametrical combination. A physical discussion in this regard is provided in Supplemental Material E [44], which also shows the coupling for the returned signals inside the power divider may happen in a lossy way [45] and causes some resistive dissipation at the general phase case $\Delta\varphi \neq m\pi$ (m being zero and positive integer).

In a reversed process, our system does not behave like any maser [46], but like a nonresonant sheet antenna that radiates plane waves toward two sides of free space. In order to excite the oscillation of the free carriers inside the film for radiation, suppose a radio-frequency voltage bias is imposed in the film plane. From the transmission line theory, an equivalent circuit consists of a driving source with internal resistance R_s from the film, and two external loads Z_0 in parallel connection accounting for two sides of free space. It is easy to prove that the condition of the maximal power gained by the loads is that the internal impedance is equal to the total external load, i.e., $R_s = Z_0/2$. Therefore, the CPA condition is closely related to the radiating performance of the ultrathin conductive sheet. This simple relation may be of great significance in optimizing the emission power of the current sheet antennas, even including THz photoconductive antennas which may be regarded as transient-current sheet and emit THz waves toward two sides of the photoconducting layer [47–49].

In technology, the absorbing layer thickness can be reduced further into nanometer scale while maintaining the sheet resistance. For example, a ∼5-nm-thick smooth Au film or a metallic mesh structure with thickness several tens of nanometers enables designing the 50% microwave absorber under single-beam illumination [50]. Such nanofilms will manifest the broadband perfect absorption at a thickness of $\sim\lambda/10^6$ for coherent illumination.

Besides the broadband nature of the film, the relative phase $\Delta\varphi = 0$ is also crucial to the frequency-independent perfect absorption. From the interference perspective, this requires experimentally a zero-path-delay interferometer for the two counterpropagating coherent beams, as done in our setup ($L = 0$). The critical condition not only guarantees the constructive interference of the E fields at the sample position to every wavelength, but also relaxes the coherence of the wave source. Thus, our results can also be observed with an incoherent source in a symmetrical setup.

IV. CONCLUSIONS

In conclusion, the broadband perfect absorption of the ultrathin conductive film is experimentally realized under coherent illumination, exhibiting structural simplicity and super performance. Two key ingredients in experiment, ultrathin profile and coherent illumination, completely eliminate the f dependency which is typically encountered in perfect absorber design, and fully liberate the inherent superiority of a simple metallic sheet by surpassing the 50% limit. Our work may enable ultrabroadband, deep subwavelength applications in microwave absorbers and antenna engineering, and bridge two important technological fields, EM absorbent materials and transparent conductors.

ACKNOWLEDGMENTS

This work was supported partly by the National Natural Science Foundation of China (Grants No. 11474212, No. 11304215, No. 11104196, and No. 11374224), the Natural Science Foundation of Jiangsu Province (Grants No. BK20141191, No. BK20130281, and No. BK2011277), and a Project Funded by the Priority Academic Program Development (PAPD) of Jiangsu Higher Education Institutions. C.W. acknowledges the support from National Research Foundation for the Doctoral Program of Higher Education of China (20103201110015). The authors thank Professor Joyce Poon, Professor Linsen Chen, Professor Xiaohong Zhou, and Professor Xinmi Yang for their help.

[1] J. D. Jackson, *Classical Electrodynamics*, 3rd ed. (Wiley, New York, 1998), Sect. 7.5.

[2] G. Nimtz and U. Panten, Broad band electromagnetic wave absorbers designed with nano-metal films, Ann. Phys. **19**, 53 (2010).

[3] C. Hilsum, Infrared absorption of thin metal films, J. Opt. Soc. Am. **44**, 188 (1954).

[4] R. C. Hansen and W. T. Pawlewicz, Effective conductivity and microwave reflectivity of thin metallic films, IEEE Trans. Microwave Theory Tech. **30**, 2064 (1982).

[5] H. Bosman, Y. Y. Lau, and R. M. Gilgenbach, Microwave absorption on a thin film, Appl. Phys. Lett. **82**, 1353 (2003).

[6] D. H. Staelin, A. W. Morgenthaler, and J. A. Kong, *Electromagnetic Waves* (Prentice-Hall, Englewood Cliffs, NJ, 1994), Sect. 4.5.

[7] B. A. Munk, *Frequency Selective Surfaces: Theory and Design* (Wiley, New York, 2000).

[8] C. M. Watts, X. Liu, and W. J. Padilla, Metamaterial electromagnetic wave absorbers, Adv. Mater. **24**, OP98 (2012).

[9] M. A. Kats, D. Sharma, J. Lin, P. Genevet, R. Blanchard, Z. Yang, M. M. Qazilbash, D. N. Basov, S. Ramanathan, and F. Capasso, Ultra-thin perfect absorber employing a tunable phase change material, Appl. Phys. Lett. **101**, 221101 (2012).

[10] M. A. Kats, R. Blanchard, P. Genevet, and F. Capasso, Nanometre optical coatings based on strong interference effects in highly absorbing media, Nat. Mater. **12**, 20 (2012).

[11] F. Qin and C. Brosseau, A review and analysis of microwave absorption in polymer composites filled with carbonaceous particles, J. Appl. Phys. **111**, 061301 (2012).

[12] Z. P. Chen, C. Xu, C. Q. Ma, W. C. Ren, and H. M. Cheng, Lightweight and flexible graphene foam composites for high-performance electromagnetic interference shielding, Adv. Mater. **25**, 1296 (2013).

[13] F. Ding, Y. X. Cui, X. C. Ge, Y. Jin, and S. L. He, Ultrabroadband microwave metamaterial absorber, Appl. Phys. Lett. **100**, 103506 (2012).

[14] Y. X. Cui, K. H. Fung, J. Xu, H. Ma, Y. Jin, S. L. He, and N. Fang, Ultrabroadband light absorption by a sawtooth anisotropic metamaterial slab, Nano Lett. **12**, 1443 (2012).

[15] N. I. Landy, S. Sajuyigbe, J. J. Mock, D. R. Smith, and W. J. Padilla, Perfect metamaterial absorber, Phys. Rev. Lett. **100**, 207402 (2008).

[16] H. Li, L. H. Yuan, B. Zhou, X. P. Shen, Q. Cheng, and T. J. Cui, Ultrathin multiband gigahertz metamaterial absorbers, J. Appl. Phys. **110**, 014909 (2011).

[17] D. X. Ye, Z. Y. Wang, K. W. Xu, H. Li, J. T. Huangfu, Z. Wang, and L. X. Ran, Ultrawideband dispersion control of a metamaterial surface for perfectly-matched-layer-like absorption, Phys. Rev. Lett. **111**, 187402 (2013).

[18] J. M. Hao, J. Wang, X. L. Liu, W. J. Padilla, L. Zhou, and M. Qiu, High performance optical absorber based on a plasmonic metamateiral, Appl. Phys. Lett. **96**, 251104 (2010).

[19] Z. Y. Liu, X. X. Zhang, Y. W. Mao, Y. Y. Zhu, Z. Y. Yang, C. T. Chan, and P. Sheng, Locally resonant sonic materials, Science **289**, 1734 (2000).

[20] J. Mei, G. C. Ma, M. Yang, Z. Y. Yang, W. J. Wen, and P. Sheng, Dark acoustic metamaterials as super absorbers for low-frequency sound, Nat. Commun. **3**, 756 (2012).

[21] N. Engheta, Thin absorbing screens using metamaterial surfaces, in *Proceedings of IEEE International Symposium on Antennas and Propagation Society*, Vol. 2 (IEEE, Piscataway, 2002), pp. 392–395.

[22] J. R. Tischler, M. S. Bradley, and V. Bulovic, Critically coupled resonators in vertical geometry using a planar mirror and a 5 nm thick absorbing film, Opt. Lett. **31**, 2045 (2006).

[23] S. Deb, S. Dutta Gupta, J. Banerji, and S. Dutta Gupta, Critical coupling at oblique incidence, J. Opt. A: Pure Appl. Opt. **9**, 555 (2007).

[24] R. L. Fante and M. T. McCormack, Reflection properties of the salisbury screen, IEEE Trans. Antennas Propag. **36**, 1443 (1988).

[25] Y. D. Chong, L. Ge, H. Cao, and A. D. Stone, Coherent perfect absorbers: Time-reversed lasers, Phys. Rev. Lett. **105**, 053901 (2010).

[26] W. J. Wan, Y. D. Chong, L. Ge, H. Noh, A. D. Stone, and H. Cao, Time-reversed lasing and interferometric control of absorption, Science **331**, 889 (2011).

[27] H. Noh, Y. D. Chong, A. D. Stone, and H. Cao, Perfect coupling of light to surface plasmons by coherent absorption, Phys. Rev. Lett. **108**, 186805 (2012).

[28] H. Noh, S. M. Popoff, and H. Cao, Broadband subwavelength focusing of light using a passive sink,Opt. Express **21**, 17435 (2013).

[29] S. Dutta Gupta, O. J. F. Martin, S. Dutta Gupta, and G. S. Agarwal, Controllable coherent perfect absorption in a composite film, Opt. Express **20**, 1330 (2012).

[30] M. B. Pu, Q. Feng, M. Wang, C. G. Hu, C. Huang, X. L. Ma, Z. Y. Zhao, C. T. Wang, and X. G. Luo, Ultrathin broadband nearly perfect absorber with symmetrical coherent illumination, Opt. Express **20**, 2246 (2012).

[31] J. F. Zhang, K. F. Macdonald, and N. I. Zheludev, Controlling light-with-light without nonlinearity, Light: Sci. Appl. **1**, e18 (2012).

[32] M. Kang, F. Liu, T.-F. Li, Q.-H. Guo, J. Li, and J. Chen, Polarization-independent coherent perfect absorption by a dipole-like metasurface, Opt. Lett. **38**, 3086 (2013).

[33] G. Ramakrishnan, G. K. P. Ramanandan, A. J. L. Adam, M. Xu, N. Kumar, R. W. A. Hendrikx, and P. C. M. Planken, Enhanced terahertz emission by coherent optical absorption in ultrathin semiconductor films on metals, Opt. Express **21**, 16784 (2013).

[34] G. Pirruccio, L. M. Moreno, G. Lozano, and J. G. Rivas, Coherent and broadband enhanced optical absorption in graphene, ACS Nano **7**, 4810 (2013).

[35] K. L. Chopraa, S. Majora, and D. K. Pandya, Transparent conductors—A status review, Thin Solid Films **102**, 1 (1983).

[36] C. G. Granqvist, Transparent conductors as solar energy materials: A panoramic review, Sol. Energy Materials and Sol. Cells **91**, 1529 (2007).

[37] R. G. Gordon, Criteria for choosing transparent conductors, MRS Bull. **25**, 52 (2000).

[38] D. S. Hecht, L. B. Hu, and G. Irvin, Emerging transparent electrodes based on thin films of carbon nanotubes, graphene, and metallic nanostructures, Adv. Mater. **23**, 1482 (2011).

[39] J. K. Wassei and R. B. Kaner, Graphene, a promising transparent conductor, Mater. Today **13**, 52 (2010).

[40] P. B. Catrysse and S. H. Fan, Nanopatterned metallic films for use as transparent conductive electrodes in optoelectronic devices, Nano Lett. **10**, 2944 (2010).

[41] X. Y. Zeng, Q. K. Zhang, R. M. Yu, and C. Z. Lu, A new transparent conductor: Silver nanowire film buried at the surface of a transparent polymer, Adv. Mater. **22**, 4484 (2010).

[42] P. Kuang, J.-M. Park, W. Leung, R. C. Mahadevapuram, K. S. Nalwa, T.-G. Kim, S. Chaudhary, K.-M. Ho, and K. Constant, A new architecture for transparent electrodes: Relieving the trade-off between electrical conductivity and optical transmittance, Adv. Mater. **23**, 2469 (2011).

[43] H. Wu, D. S. Kong, Z. C. Ruan, P.-C. Hsu, S. Wang, Z. F. Yu, T. J. Carney, L. B. Hu, S. H. Fan, and Y. Cui, A transparent electrode based on a metal nanotrough network, Nat. Nanotech. **8**, 421 (2013).

[44] See Supplemental Material at http://link.aps.org/supplemental/10.1103/PhysRevB.91.220301 for some details including samples, microwave measurements, theoretical calculations, EM parameters, and the discussion about the twin absorption peaks.

[45] D. M. Pozar, *Microwave Engineering*, 2nd ed. (Wiley, New York, 1998), Sect. 7.3. The power divider (broadband Wilkinson type) is lossless when the returned signals at two equal-split ports are in phase and have identical magnitude, or else it becomes absorptive owing to the unbalanced internal resistor. The lossy situation happens only in the coherent control of absorption with the relative phase value $\Delta\varphi \neq m\pi$ (m being zero and positive integer) for our experiments and the referred absorbance consists of both the film's and the divider's contribution in such situation, as discussed in Supplemental Material E [44]. When $\Delta\varphi = m\pi$, with which we are mainly concerned, the device performs no loss and only the film matters (maximal or zero absorption depending on m).

[46] J. P. Gordon, H. J. Zeiger, and C. H. Townes, The maser—New type of microwave amplifier, frequency standard, and spectrometer, Phys. Rev. **99**, 1264 (1955).

[47] X. C. Zhang and J. Xu, *Introduction to THz Wave Photonics* (Springer, New York, 2010).

[48] Y. S. Lee, *Principles of Terahertz Science and Technology* (Springer, New York, 2009).

[49] In fact, the THz photoconductive antenna may be regarded as the radiating current sheet, where the photocarriers generated in the optically absorbing layer of the semiconductors upon illumination by the femtosecond laser pulse and driven by a voltage bias emit THz waves toward two sides of space.

[50] S. C. Li, S. Anwar, W. X. Lu, Z. H. Hang, B. Hou, M. R. Shen, and C.-H. Wang, Microwave absorptions of ultrathin conductive films and designs of frequency-independent ultrathin absorbers, AIP Adv. **4**, 017130 (2014).